

We are IntechOpen, the world's leading publisher of Open Access books Built by scientists, for scientists

4,800

Open access books available

122,000

International authors and editors

135M

Downloads

Our authors are among the

154

Countries delivered to

TOP 1%

most cited scientists

12.2%

Contributors from top 500 universities



WEB OF SCIENCE™

Selection of our books indexed in the Book Citation Index
in Web of Science™ Core Collection (BKCI)

Interested in publishing with us?
Contact book.department@intechopen.com

Numbers displayed above are based on latest data collected.

For more information visit www.intechopen.com



The KCLBOT: A Framework of the Nonholonomic Mobile Robot Platform Using Double Compass Self-Localisation

Evangelos Georgiou, Jian Dai and Michael Luck
*King's College London
United Kingdom*

1. Introduction

The key to effective autonomous mobile robot navigation is accurate self-localization. Without self-localization or with inaccurate self-localization, any non-holonomic autonomous mobile robot is blind in a navigation environment. The KCLBOT [1] is a non-holonomic two wheeled mobile robot that is built around the specifications for 'Micromouse Robot' and the 'RoboCup' competition. These specifications contribute to the mobile robot's form factor and size. The mobile robot holds a complex electronic system to support on-line path planning, self-localization, and even simultaneous localization and mapping (SLAM), which is made possible by an onboard sensor array. The mobile robot is loaded with eight Robot-Electronics SRF05 [2] ultrasonic rangefinders, and its drive system is supported by Nubotics WC-132 [3] WheelCommander Motion Controller and two WW-01 [4] WheelWatcher Encoders. The motors for robot are modified continuous rotation servo motors, which are required for the WheelCommander Motion Controller. The rotation of the mobile robot is measured by Robot-Electronics CMPS03 [5] Compass Module. These two modules make the double compass configuration, which supports the self-localization theory presented in this paper. Each individual module provides the bearing of the mobile robot relative to the magnetic field of the earth. The central processing for the mobile robot is managed by a Savage Innovations OOPic-R microcontroller. The OOPic-R has advanced communication modules to enable data exchange between the sensors and motion controller. Communication is managed via a serial bus and an I²C bus. The electronics are all mounted on two aluminium bases, which make the square structure of the mobile robot. To support the hardware requirements of the novel localisation methodology, the cutting edge technology of a 200 MHz 32-bit ARM 9 processor on a GHI ChipworkX module [6] is employed. The software architecture is based on the Microsoft .NET Micro Framework 4.1 using C# and the Windows Presentation Foundation (WPF).

The combination of hardware electronics and drive mechanics, makes the KCLBOT, as represented in Fig. 1, a suitable platform for autonomous self-localization.

Many different systems have been considered for self-location, from using visual odometry [7] to using a GPS method. While all of these have benefits and detriments, the solution

proposed in this paper endeavours to offer significantly more benefits than detriments. Over the years, several solutions to self-localization have been presented. The most common application uses the vehicle's shaft encoders to estimate the distance travelled by the vehicle and deduce the position. Other applications use external reference entities to compute the vehicle's position, like global positioning systems (GPS) or marker beacons. All of these applications come with their respective weaknesses; for example, the shaft encoder assumes no slippage and is subject to accumulative drift; the GPS will not work indoors and is subject to a large margin of accuracy; and the beacons method is subject to the loss of the multi-path component delivery and accuracy is affected by shadowing, fast/slow fading, and the Doppler effect. More accurate applications have been presented using visual odometry but such applications require off-line processing or high computation time for real-time applications. Frederico et al. [8] present an interesting self-localization concept for the Bulldozer IV robot using shaft encoders, an analog compass, and optical position sensor from the PC mouse. This configuration of the vehicle is dependent on a flat surface for visual odometry to be effective; any deviation from the surface will cause inaccuracy. Hofmeister et al. [9] present a good idea for self-localization using visual odometry with a compass to cope with the low resolution visual images. While this is a very good approach to self-localization, the vehicle is dependent on a camera and the computation ability to process images quickly. Haverinen et al. [10] propose an excellent basis for self-localization utilizing ambient magnetic fields for indoor environments, whilst using the Monte Carlo Localization technique.

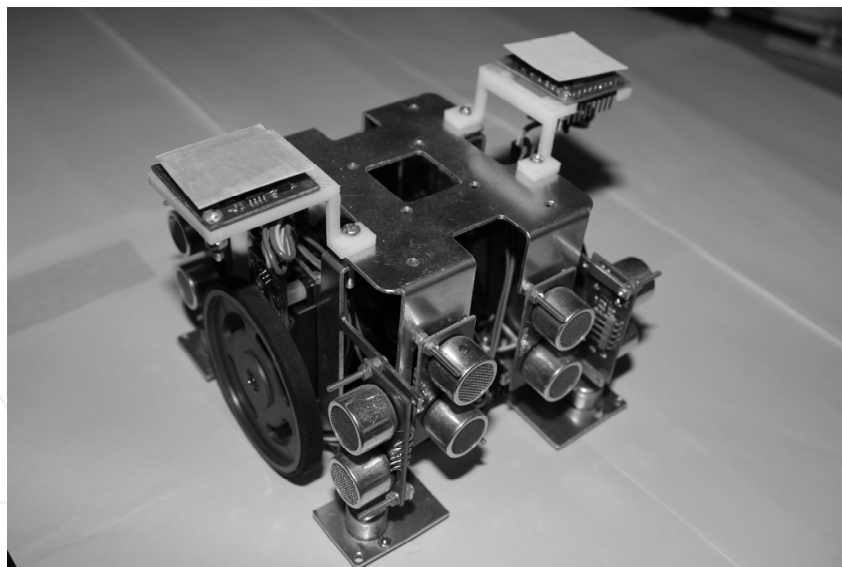


Fig. 1. The KCLBOT: A Nonholonomic Manoeuvrable Mobile Robot

It is not ideal to have multiple solutions to the position and orientation of the mobile robot and the computational requirement will affect the ability of the solution being available in real-time. Heavy computation also affects the battery life of the mobile robot and this is a critical aspect. In the technique utilizing two compasses, an analytical calculation model is presented over a numerical solution, which allows for minimal computation time over the numerical model. The configuration of the mobile robot employs two quadrature shaft encoders and two digital magnetic compasses to compute the vehicle's position and angular

orientation on a two dimensional Cartesian plane. The accuracy of analytical model is benchmarked against visual odometry telemetry. However, this model still suffers from accumulative drift because of the utilization of quadrature shaft encoders. The digital compasses also encounter the same problem with the level of resolution being limited. The ideal solution will not have accumulation of drift error and will not be dependent on the previous configuration values of position and orientation. Such a solution is only available via visual odometry.

2. A manoeuvrable nonholonomic mobile robot

In this section, the experimental vehicle is evaluated by defining its constraints and modelling its kinematic and dynamic behaviour. The constraints are based on holonomic and nonholonomic behaviour of the rotating wheels, and the vehicles pose in a two dimensional Cartesian plane. The equations of motion for the mobile robot are deduced using Lagrangian d'Alembert's principle, with the implementation of Lagrangian multiplier for optimization. The behaviour of the dual motor configuration is deduced using a combination of Newton's law with Kirchhoff's law.

2.1 Configuration constraints and singularities

In the manoeuvrable classification of mobile robots [11], the vehicle is defined as being constrained to move in the vehicle's fixed heading angle. For the vehicle to change manoeuvre configuration, it needs to rotate about itself.

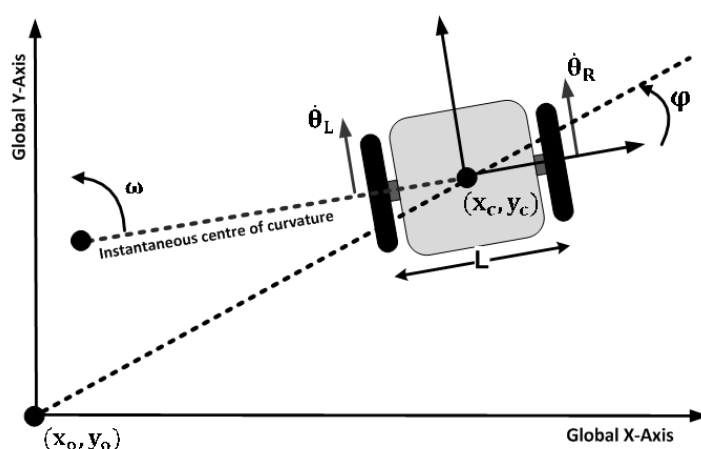


Fig. 2. A typical two wheel mobile robot constrained under the maneuverable classification.

As the vehicle traverses the two dimensional plane, both left and right wheels follow a path that moves around the instantaneous centre of curvature at the same angle, which can be defined as ω , and thus the angular velocity of the left and right wheel rotation can be deduced as follows:

$$\dot{\theta}_L = \omega \left(icc_r - \frac{L}{2} \right) \quad (1)$$

$$\dot{\theta}_R = \omega \left(icc_r + \frac{L}{2} \right) \quad (2)$$

where L is the distance between the centres of the two rotating wheels, and the parameter icc_r is the distance between the mid-point of the rotating wheels and the instantaneous centre of curvature. Using the velocities equations (1) and (2) of the rotating left and right wheels, $\dot{\theta}_L$ and $\dot{\theta}_R$ respectively, the instantaneous centre of curvature, icc_r , and the curvature angle, ω can be derived as follows:

$$icc_r = \frac{L(\dot{\theta}_R + \dot{\theta}_L)}{2(\dot{\theta}_R - \dot{\theta}_L)} \quad (3)$$

$$\omega = \frac{(\dot{\theta}_R - \dot{\theta}_L)}{L} \quad (4)$$

Using equations (3) and (4), two singularities can be identified. When $\dot{\theta}_R = \dot{\theta}_L$, the radius of instantaneous centre of curvature, icc_r tends towards infinity and this is the condition when the mobile robot is moving in a straight line. When $\dot{\theta}_R = -\dot{\theta}_L$, the mobile robot is rotating about its own centre and the radius of instantaneous centre of curvature, icc_r , is null. When the wheels on the mobile robot rotate, the quadrature shaft encoder returns a counter tick value; the rotation direction of the rotating wheel is given by positive or negative value returned by the encoder. Using the numbers of tick counts returned, the distance travelled by the rotating left and right wheel can be deduced in the following way:

$$d_L = \frac{L_{ticks}\pi D}{L_{res}} \quad (5)$$

$$d_R = \frac{R_{ticks}\pi D}{R_{res}} \quad (6)$$

where L_{ticks} and R_{ticks} depicts the number of encoder pulses counted by left and right wheel encoders, respectively, since the last sampling, and D is defined as the diameter of the wheels. With resolution of the left and right shaft encoders L_{res} and R_{res} , respectively, it is possible to determine the distance travelled by the left and right rotating wheel, d_L and d_R . This calculation is shown in equations (5) and (6).

In the field of robotics, holonomicity [12] is demonstrated as the relationship between the controllable and total degrees of freedom of the mobile robot, as presented by the mobile robot configuration in Fig. 3. In this case, if the controllable degrees of freedom are equal to the total degrees of freedom, then the mobile robot is defined as holonomic. Otherwise, if the controllable degrees of freedom are less than the total degrees of freedom, it is nonholonomic. The manoeuvrable mobile robot has three degrees of freedom, which are its position in two axes and its orientation relative to a fixed heading angle. This individual holonomic constraint is based on the mobile robot's translation and rotation in the direction of the axis of symmetry and is represented as follows:

$$\dot{y}_c \cos(\phi) - \dot{x}_c \sin(\phi) - d\dot{\phi} = 0 \quad (7)$$

where, x_c and y_c are Cartesian-based coordinates of the mobile robot's centre of mass, which is defined as P_c , and ϕ describes the heading angle of the mobile robot, which is

referenced from the global x-axis. To conclude, Equation (7) presents the pose of the mobile robot. The mobile robot has two controllable degrees of freedom, which control the rotational velocity of the left and right wheel and, adversely – with changes in rotation – the heading angle of the mobile robot is affected; these constraints are stated as follows:

$$\dot{y}_c \sin(\phi) + \dot{x}_c \cos(\phi) + L\dot{\phi} = r\dot{\theta}_r \tag{8}$$

$$\dot{y}_c \sin(\phi) + \dot{x}_c \cos(\phi) - L\dot{\phi} = r\dot{\theta}_l \tag{9}$$

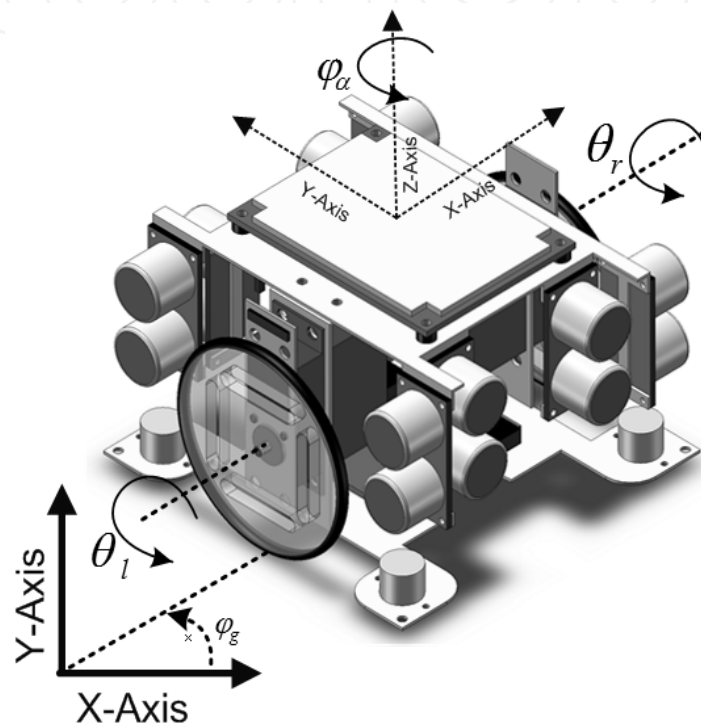


Fig. 3. A Manoeuvrable Nonholonomic mobile robot

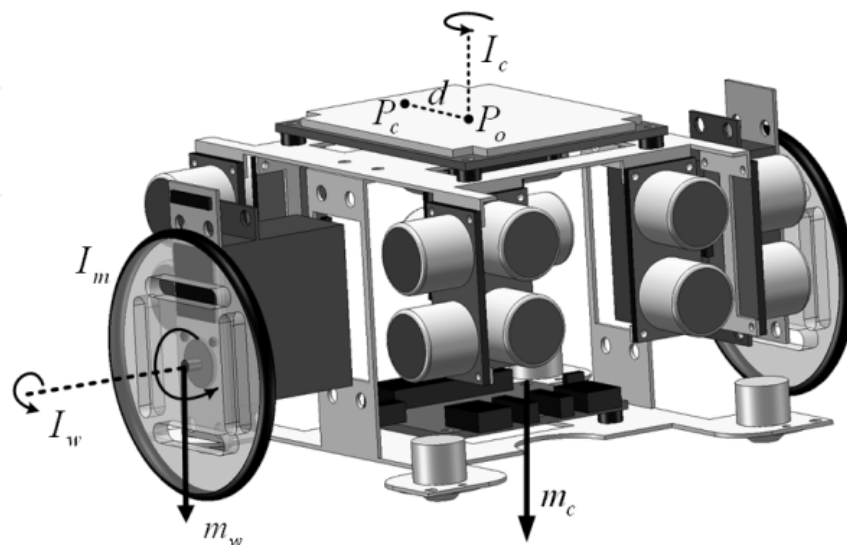


Fig. 4. The Mobile Robot Drive Configuration

where $\dot{\theta}_r$ and $\dot{\theta}_l$ are the angular displacements of the right and left mobile robot wheels, respectively, and where r describes the radius of the mobile robot's driving wheels. As such, the two-wheeled manoeuvrable mobile robot is a nonholonomic system. To conclude, Equation (8) and (9) describe the angular velocity of the mobile robot's left and right wheel.

Symbol	Description of Structured Constant
P_o	The intersection of the axis of symmetry with the mobile robot's driving wheel axis
P_c	The centre of the mass of the mobile robot
d	The distance between P_o and P_c
I_c	The moment of inertia of the mobile robot without the driving wheels and the rotating servo motors about a vertical axis through P_o
I_w	The moment of inertia of each of the wheels and rotating servo motors about the wheel's axis
I_m	The moment of inertia of each of the wheels and rotating servo motors about the diameter of the wheels
m_c	The mass of the mobile robot without the driving wheels and the rotating servo motors
m_w	The mass of each of the mobile robot's wheels and rotating motors

Table 1. The Mobile Robots Constants

Based on the mobile robot drive configuration, presented in Fig. 4., Table 1 describes the structured constants required to provide the physical characteristics of the mobile robots movement.

2.2 Kinematics a dynamics modeling

Using the diagrammatic model expressed by Figures 2 and 3, and the structured constants listed in Table 1, the nonholonomic equations of motion with Lagrangian multiplier are derived using Lagrange - d'Alembert's principle [13] and are specified as follows:

$$M(q)\ddot{q} + V(q, \dot{q}) + G(q) = E(q)u + B^T(q)\lambda_n \quad (10)$$

where $M(q)$ describes an $n \times n$ dimensional inertia matrix, and where $M(q)\ddot{q}$ is represented as follows:

$$\begin{bmatrix} (m_c + 2m_w) & 0 & -m_c d \ddot{\phi} \sin(\phi) & 0 & 0 \\ 0 & (m_c + 2m_w) & m_c d \ddot{\phi} \cos(\phi) & 0 & 0 \\ -m_c d \sin(\phi) & m_c d \cos(\phi) & I_z & 0 & 0 \\ 0 & 0 & 0 & I_w & 0 \\ 0 & 0 & 0 & 0 & I_w \end{bmatrix} \begin{bmatrix} \ddot{x}_c \\ \ddot{y}_c \\ \ddot{\phi}_c \\ \ddot{\theta}_r \\ \ddot{\theta}_l \end{bmatrix} \quad (11)$$

Here, $I_z = (I_c + 2m_w(d^2 + L^2) + 2I_m)$ and $V(q, \dot{q})$ describes an n dimensional velocity dependent force vector and is represented as follows:

$$\begin{bmatrix} -m_c d \dot{\phi}^2 \cos(\phi) \\ -m_c d \dot{\phi}^2 \sin(\phi) \\ 0 \\ 0 \\ 0 \end{bmatrix} \quad (12)$$

$G(q)$ describes the gravitational force vector, which is null and is not taken into consideration, u describes a vector of r dimensions of actuator force/torque, $E(q)$ describes an $n \times r$ dimensional matrix used to map the actuator space into a generalized coordinate space, and $E(q)u$ is specified as follows:

$$\begin{bmatrix} 0 & 0 \\ 0 & 0 \\ 0 & 0 \\ 1 & 0 \\ 0 & 1 \end{bmatrix} \begin{bmatrix} \tau_r \\ \tau_l \end{bmatrix} \quad (13)$$

Where the expression is in terms of coordinates (q, \dot{q}) where $q \in \mathbb{R}^n$ is the position vector and $\dot{q} \in \mathbb{R}^n$ is the velocity vector. Where q is defined as $[x_c, y_c, \phi, \theta_r, \theta_l]^T$, the constraints equation can be defined as $A(q)\dot{q} = 0$. Where, $A(q)$, the constraints matrix is expressed as follows:

$$A(q)\dot{q} = \begin{bmatrix} -\sin(\phi) & \cos(\phi) & -d & 0 & 0 \\ -\cos(\phi) & -\sin(\phi) & -b & r & 0 \\ -\cos(\phi) & -\sin(\phi) & b & 0 & r \end{bmatrix} \begin{bmatrix} \dot{x}_c \\ \dot{y}_c \\ \dot{\phi} \\ \dot{\theta}_r \\ \dot{\theta}_l \end{bmatrix} \quad (14)$$

Where finally, $B^T(q) = A^T(q)$ and λ_n describes an m dimensional vector of Lagrangian multipliers and can be described as follows:

$$\begin{bmatrix} -\sin(\phi) & -\cos(\phi) & -\cos(\phi) \\ \cos(\phi) & -\sin(\phi) & -\sin(\phi) \\ -d & -L & L \\ 0 & r & 0 \\ 0 & 0 & r \end{bmatrix} \begin{bmatrix} \lambda_1 \\ \lambda_2 \\ \lambda_3 \end{bmatrix} \quad (15)$$

The purpose of using the Lagrangian multipliers is to optimize the behaviour of the nonholonomic manoeuvrable mobile robot, by providing a strategy for finding the maximum or minimum of the equations' behaviour, subject to the defined constraints.

Equation (10) describes the Lagrangian representation of the KCLBOT, in a state-space model, and Equations (11), (12), (13), (14), and (15) decompose the state-space model.

2.3 The dual-drive configuration

The manoeuvrable mobile robot is configured with two independent direct current (DC) servo motors, set up to be parallel to each other, with the ability for continuous rotation. This configuration allows the mobile robot to behave in a manoeuvrable configuration, is illustrated in Figure 5.

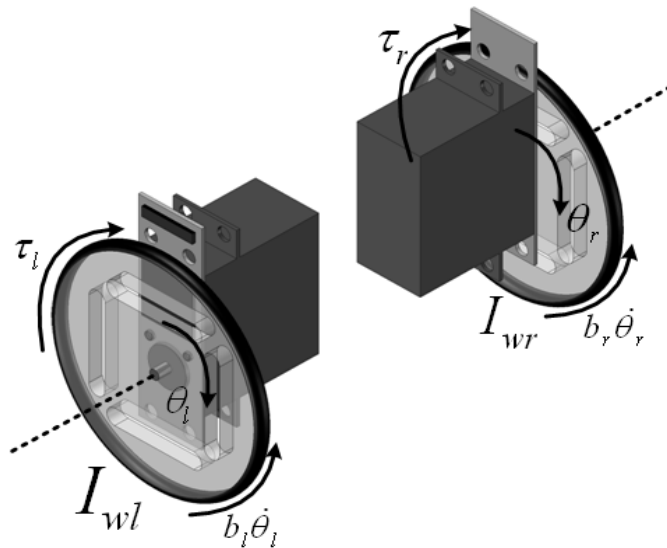


Fig. 5. Dual Servo Motor Drive Configuration

It is assumed that both the left and right servo motors are identical. The torque, $\tau_{l,r}$, of the motor is related to the armature current, $i_{l,r}$, by the constant factor K_t and is described as $\tau_{l,r} = K_t \cdot i_{l,r}$. The input voltage source is described as $V_{l,r}$, which is used to drive the servo motors, where $R_{l,r}$ is internal resistance of the motor, $L_{l,r}$ is the internal inductance of the motor, and $e_{l,r}$ describes back electromagnetic field (EMF) of both the left and right electric servo motors. It is known that $e_{l,r} = K \cdot \theta_{l,r}$, where $K = K_e = K_t$ describe the electromotive force constants.

Symbol	Description
$I_{wl,r}$	Moment of inertia of the rotor
$b_{l,r}$	Damping ratio of the mechanical system
K	Electromotive force constant
$R_{l,r}$	Electric resistance
$L_{l,r}$	Electric inductance
$V_{l,r}$	Input voltage source

Table 2. Dual Servo Motor Configuration Value Definitions

The value definitions listed in Table 2 complement Fig. 5's representation of the mobile robot drive configuration.

Using Newton's laws of motion and Kirchhoff's circuit laws [14], the motion of the motors can be related to the electrical behaviour of the circuit.

$$I_{wl,r}\ddot{\theta}_{l,r} + b_{l,r}\dot{\theta}_{l,r} = K i_{l,r} \quad (16)$$

$$L_{l,r} \frac{di_{l,r}}{dt} + R_{l,r} i_{l,r} = V_{l,r} - K \dot{\theta}_{l,r} \quad (17)$$

Equation (16) specifies the Newtonian derivation of motion of both motors and equation (17) specifies how the circuit behaves applying Kirchhoff's laws. Having derived equations (16) and (17), the next step is to relate the electrical circuit behaviour to the mechanical behaviour of rotating motors, and this is achieved using Laplace transforms and expressing equations (16) and (17) in terms of s as follows:

$$\frac{\dot{\theta}}{V_{l,r}} = \frac{K}{(I_{wl,r}s + b_{l,r})(L_{l,r}s + R_{l,r}) + K^2} \quad (18)$$

$$(L_{l,r}s + R_{l,r})I_{l,r}(s) = V_{l,r} - Ks\theta_{l,r}(s) \quad (19)$$

Using equations (18) and (19), the open-loop transfer function of this configuration can be derived by eliminating $I_{l,r}(s)$ and relating the equation of motion to the circuit behaviour as follows:

$$\frac{\dot{\theta}}{V_{l,r}} = \frac{K}{(I_{wl,r}s + b_{l,r})(L_{l,r}s + R_{l,r}) + K^2} \quad (20)$$

Here, equation (20) equates the rotational speed of the motors as the systems output and the voltage applied to the motors as the systems input.

In summary, the constraints of the experimental vehicle have been derived in equations (7), (8), and (9), in both holonomic and nonholonomic forms. Using the system constraints, the behaviour of the nonholonomic manoeuvrable mobile robot is formed using the Lagrange-d'Alembert principle with Lagrangian multipliers to optimize the performance of the system, as specified in equations (10), (11), (12), (13), (14), and (15). Finally, using Newton's laws of motion and Kirchhoff's laws to evaluate circuits, a model is derived using Laplace transforms, to relate the behaviour of the systems motion to the electrical circuit.

3. Manoeuvrable mobile robot self-localization

The self-localization offers a different approach to solving for an object's position. The reason for the perpetuation of so many approaches is that no solution has yet offered an absolutely precise solution to position. In the introduction, three major approaches using the shaft encoder telemetry, using the visual odometry, and using the global position system were discussed, of which all three have inherent problems. This paper, hence, proposes an alternative approach, which is a hybrid model using the vehicle's dual shaft encoders and double compass configuration.

3.1 Implementing a dual-shaft encoder configuration

By using the quadrature shaft encoders that accumulate the distance travelled by the wheels, a form of position can be deduced by deriving the mobile robot's x , y Cartesian position and the manoeuvrable vehicle's orientation ϕ , with respect to time. The derivation starts by defining and considering $s(t)$ and $\phi(t)$ to be function of time, which represents the velocity and orientation of the mobile robot, respectively. The velocity and orientation are derived from differentiating the position form as follows:

$$\frac{dx}{dt} = s(t) \cdot \cos(\phi(t)) \quad (21)$$

$$\frac{dy}{dt} = s(t) \cdot \sin(\phi(t)) \quad (22)$$

The change in orientation with respect to time is the angular velocity ω , which was defined in equation (4) and can be specified as follows:

$$\frac{d\phi}{dt} = \omega = \frac{\dot{\theta}_r - \dot{\theta}_l}{b} \quad (23)$$

When equation (23) is integrated, the mobile robot's angle orientation value $\phi(t)$ with respect to time is achieved. The mobile robot's initial angle of orientation $\phi(0)$ is written as ϕ_0 and is represented as follows:

$$\phi(t) = \frac{(\dot{\theta}_r - \dot{\theta}_l)t}{b} + \phi_0 \quad (24)$$

The velocity of the mobile robot is equal to the average speed of the two wheels and this can be incorporated into equations (21) and (22), as follows:

$$\frac{dx}{dt} = \frac{\dot{\theta}_r + \dot{\theta}_l}{2} \cos(\phi(t)) \quad (25)$$

$$\frac{dy}{dt} = \frac{\dot{\theta}_r + \dot{\theta}_l}{2} \sin(\phi(t)) \quad (26)$$

The next step is to integrate equations (25) and (26) to the initial position of the mobile robot, as follows:

$$x(t) = x_0 + \frac{L(\dot{\theta}_r + \dot{\theta}_l)}{2(\dot{\theta}_r - \dot{\theta}_l)} \left(\sin\left(\frac{(\dot{\theta}_r - \dot{\theta}_l)t}{b} + \phi_0\right) - \sin(\phi_0) \right) \quad (27)$$

$$y(t) = y_0 + \frac{L(\dot{\theta}_r + \dot{\theta}_l)}{2(\dot{\theta}_r - \dot{\theta}_l)} \left(\cos\left(\frac{(\dot{\theta}_r - \dot{\theta}_l)t}{b} + \phi_0\right) - \cos(\phi_0) \right) \quad (28)$$

Equations (27) and (28) specify the mobile robot's position, where $x(0) = x_0$ and $y(0) = y_0$ are the mobile robot's initial positions. The next step is to represent equations (24), (27) and

(28) in terms of the distances that the left and right wheels have traversed, which are defined by d_R and d_L . This can be achieved by substituting $\dot{\theta}_r$ and $\dot{\theta}_l$ (in equations (24), (27) and (28)) for d_R and d_L , respectively, and also dropping the time constant t to achieve the following:

$$\theta = \frac{d_R - d_L}{2} + \theta_0 \tag{29}$$

$$x(t) = x_0 + \frac{L(d_R + d_L)}{2(d_R - d_L)} \left(\sin\left(\frac{(d_R - d_L)t}{b} + \phi_0\right) - \sin(\phi_0) \right) \tag{30}$$

$$y(t) = y_0 + \frac{L(d_R + d_L)}{2(d_R - d_L)} \left(\cos\left(\frac{(d_R - d_L)t}{b} + \phi_0\right) - \cos(\phi_0) \right) \tag{31}$$

By implementing equations (29), (30), and (31), we provide a solution to the relative position of a manoeuvrable mobile robot. This might offer a possible solution to the self-localization problem but is subject to accumulative drift of the position and orientation with no method of re-alignment. The accuracy of this method is subject to the sampling rate of the data accumulation, such that if small position or orientation changes are not recorded, then the position and orientation will be erroneous.

3.2 Numerical approach with a single compass configuration

Having derived a self-localization model using only the telemetry from the quadrature shaft encoders, the next step to evolve the model is to add a digital compass to input the manoeuvrable mobile robot's orientation. The ideal position on the vehicle for the digital compass would be at the midpoint between its centre of its mass and the intersection of the axis of symmetry with the mobile robot's driving wheel axis. In this case, the vehicle is configured such that there is no deviation between the two points, P_o and P_c .

When the manoeuvrable mobile robot starts a forward or backward rotation configuration, it induces two independent instantaneous centres of curvatures from the left and right wheel. The maximum arcs of the curvature lines are depicted in Fig. 9, showing the steady state changes to the configuration as it rotates.

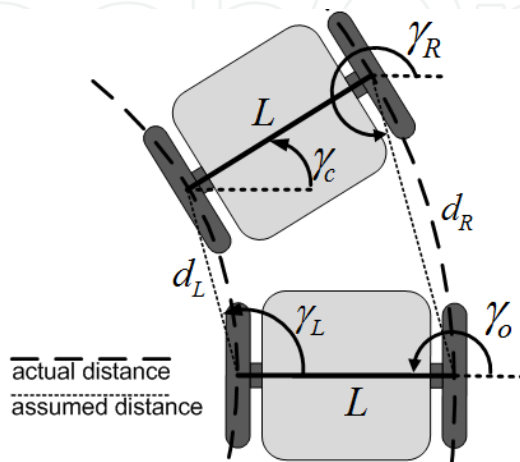


Fig. 6. Mobile Robot Manoeuvre Configuration

Using a steady state manoeuvre, it is assumed that the actual distance travelled in a rotation manoeuvre does not equal the distance used to model the calculation for position and orientation. This assumption is depicted in Fig. 6., clearly showing the actual and assumed distance travelled. The difference does not cause any consequence to the calculation model as the difference cannot be measured in the resolution of the quadrature shaft encoders.

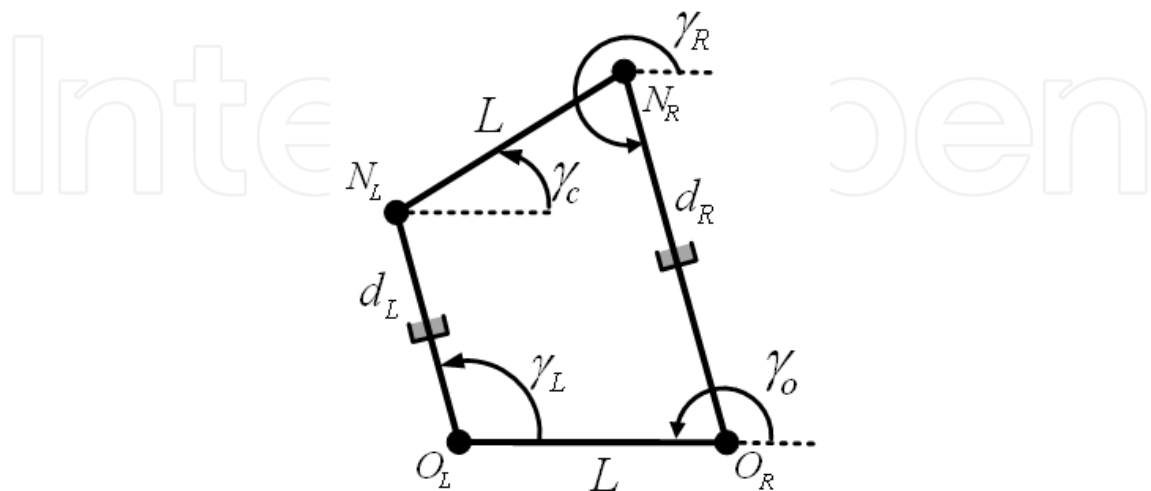


Fig. 7. Six-bar Linkage Manoeuvre Model with a Single Compass Configuration

Using the vector loop technique [15] to analyse the kinematic position of the linkage model in Fig. 7., the vector loop equation is written as follows:

$$I_{N_L O_L} + I_{N_R N_L} + I_{O_R N_R} + I_{O_L O_R} = 0 \quad (32)$$

Using the complex notation, equation (32) is written as follows:

$$d_L e^{j\gamma_L} + L e^{j\gamma_c} + d_R e^{j\gamma_R} + L e^{j\gamma_o} = 0 \quad (33)$$

Having derived the complex notation of the vector loop equation in equation (33), the next step is to substitute the Euler equations to the complex notations as follows:

$$d_L (\cos(\gamma_L) + j \sin(\gamma_L)) + L (\cos(\gamma_c) + j \sin(\gamma_c)) + d_R (\cos(\gamma_R) + j \sin(\gamma_R)) + L (\cos(\gamma_o) + j \sin(\gamma_o)) = 0 \quad (34)$$

Equation (34) is separated into its corresponding real and imaginary parts, considering $\gamma_o = 180^\circ$, as follows:

$$d_L \cos(\gamma_L) + L \cos(\gamma_c) + d_R \cos(\gamma_R) - L = 0 \quad (35)$$

$$d_L \sin(\gamma_L) + L \sin(\gamma_c) + d_R \sin(\gamma_R) = 0 \quad (36)$$

where, d_L , d_R , and L are all known constants, and γ_c specifies the new angle of orientation of the mobile robot. Having two equations (35) and (36), with two unknown angles γ_L and γ_R , when solving simultaneously for these two angles, it will return multiple independent values. This approach requires a large amount of computation to first find these angles and then deduce the relative position.

3.3 Double compass configuration methodology

Having described the issues associated with using a single compass to solve for the position above, it is clear that it would be preferable to have a model that eliminated having simultaneous solutions and led to a single solution. This would ideally mean that the angles γ_L and γ_R are known constants, and to achieve this condition requires additional telemetry from the vehicle. A model with dual compasses is proposed to resolve the angles γ_L and γ_R , as shown in Fig. 8.

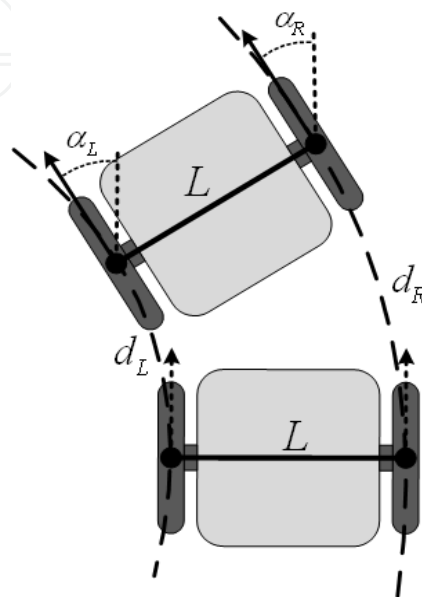


Fig. 8. Double Compass Manoeuvre Configuration

By introducing two compasses, which are placed directly above the rotating wheels, when a configuration change takes place, the difference is measured by α_L and α_R , which represent the change in orientation of the left and right mobile robot wheels, respectively. Using the same approach as a single compass configuration, the double compass manoeuvre configuration is modelled using a six-bar mechanism as shown in Fig. 9.

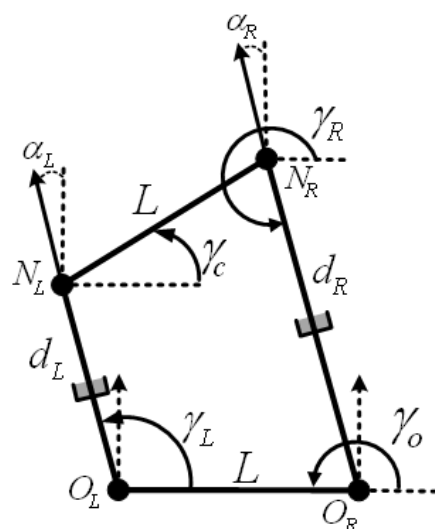


Fig. 9. Six-bar Linkage Manoeuvre Model with a Double Compass Configuration

Using an identical approach as the single compass configuration, the vector loop equations remain the same, equations (35) and (36), with the difference being the ability to define the angles γ_L and γ_R . For this manoeuvre model, presented in Fig. 9., the configuration can be calculated as follows:

$$\gamma_L = \beta_L + \alpha_L \quad (37)$$

$$\gamma_R = \beta_R + \alpha_R \quad (38)$$

where, β_L and β_R are the trigonometric angles used for calculating γ_L and γ_R for each pose of the mobile robot, based on the different configuration states of d_L and d_R . For the configuration state described by Fig. 13, $\beta_L = 90^\circ$ and $\beta_R = 270^\circ$. Having a constant value for the angles γ_L and γ_R from Equations (37) and (38), it allows either equation (35) or (36) to be used to derive the remaining angle γ_c , which is specified as follows:

$$\gamma_c = \cos^{-1} \left(\frac{-d_L \cos(\gamma_L) - d_r \cos(\gamma_R) + L}{L} \right) \quad (39)$$

$$\gamma_c = \sin^{-1} \left(\frac{-d_L \sin(\gamma_L) - d_r \sin(\gamma_R)}{L} \right) \quad (40)$$

where equations (39) and (40) solve the single compass solution to the position of the centrally positioned digital compass, indicated by γ_c .

Using the simultaneous solutions from comparing equations (35) and (36), and evaluating their difference to either equation (39) or (40), it is possible to derive the accuracy of the measurement. The simultaneous equation solution will be the best fit model for the hybrid model and any ambiguity can be considered resolution error or a factor of wheel slippage.

4. Mobile robot localization using visual odometry

4.1 Implementing visual odometry with an overhead camera

Using any standard camera at a resolution of 320 by 240 pixels, the system uses this device to capture images that are then used to compute the position and orientation of the manoeuvring mobile robot.

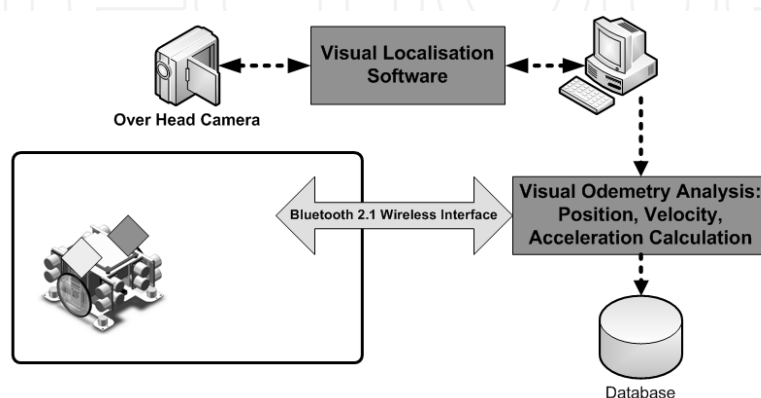


Fig. 10. Localization Configuration Setup

The camera is positioned above the manoeuvrable mobile robot at a fixed height. The camera is connected to an ordinary desktop computer that processes the images captured from the camera. The captured images are then processed to find the two markers on the mobile robot. The markers are positioned directly above the mobile robot's rolling wheels. The processing software then scans the current image identifying the marker positions. Having two markers allows the software to deduce the orientation of the manoeuvring mobile robot. When the software has deduced the position and orientation of the mobile robot, this telemetry is communicated to the mobile robot via a wireless Bluetooth signal.

4.2 A skip-list inspired searching algorithm

By using a systematic searching algorithm, the computation cost-time is dependent on the location of the markers. The closer the markers are to the origin (e.g. coordinates (0 pixels, 0 pixels) of the search, the faster the search for the markers will be performed. The systematic search algorithm is represented as follows:

```
For x-pixel = 0 To Image width
  For y-pixel = 0 To Image height
    If current pixel (x-pixel, y-pixel) = Marker 1 Then
      Marker 1 x position = x-pixel
      Marker 1 y position = y-pixel
      Flag = Flag + 1
    End if
    If current pixel (x-pixel, y-pixel) = Marker 2 Then
      Marker 2 x position = x-pixel
      Marker 2 y position = y-pixel
      Flag = Flag + 1
    End if
    If Flag > 1 Then
      x-pixel = Image width
      y-pixel = Image height
    End if
  Next
Next
```

The search algorithm above shows how every vertical and horizontal pixel is scanned to identify the two defined markers on the mobile robot. When a marker is found, a flag is raised, and when the search has two raised flags, the search will end.

5. Results & analysis

5.1 Statistical results

To validate the double compass approach to self-localisation, an overhead camera visual odometry tracking system was set up, as presented in the previous section. The visual tracking results are used to compare the double compass tracking results.

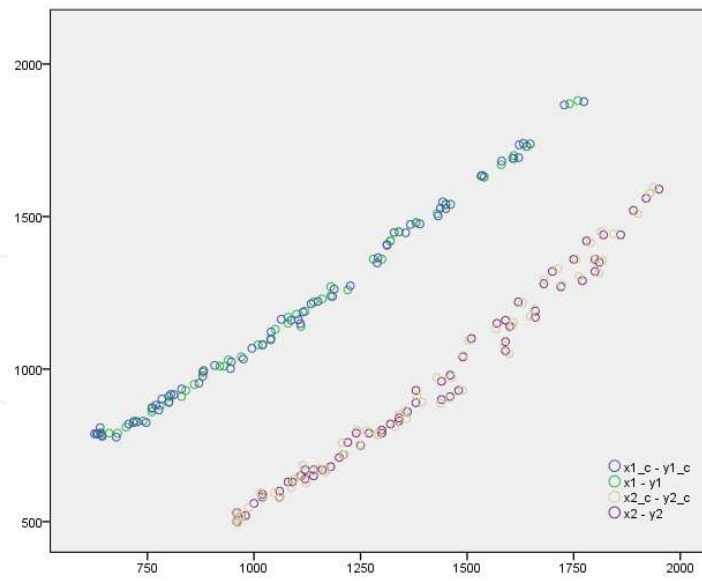


Fig. 11. Experimental data from linear path following

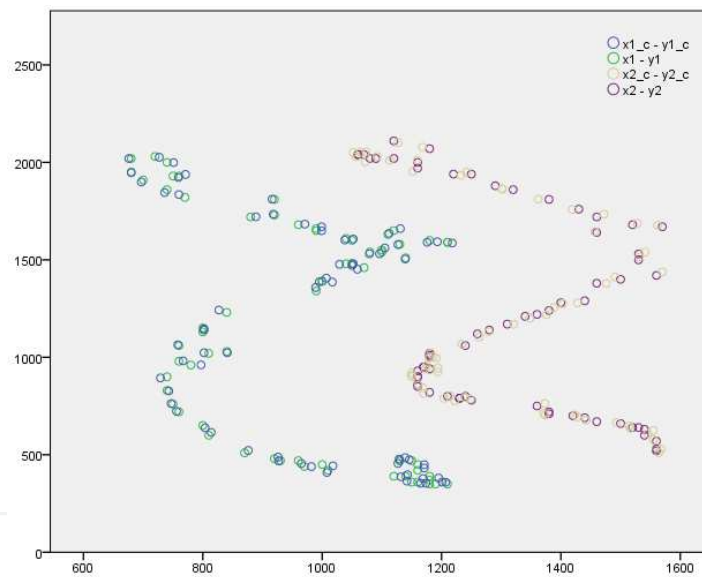


Fig. 12. Experimental data from sinusoidal path following

Using the configuration presented in Fig. 10, the mobile robot with a double compass configuration was set up to follow a linear path and a sinusoidal path. The experimental results showing the visual tracking results and the double compass estimation results are presented in Fig. 11, and Fig. 12.

The results presented in Table 3 show the statistical analyses of 362 samples recorded from the linear and sinusoidal manoeuvre experiments. Both left and right marker mean values are relatively low and, for more accuracy, because the data might be skewed, the median value is presented because it compensates for skewed data. The confidence intervals, which represent two standard deviations from the mean, equivalently present a low error rate.

Method	Right Marker	Left Marker
Mean	12.298302	11.254462
95% Confidence Interval for Mean (LB)	11.605941	10.616642
95% Confidence Interval for Mean (UB)	12.990663	11.892282
Median	12.806248	11.401754
Variance	22.284	18.911
Standard Deviation	4.7205636	4.3486990
Standard Error Mean	0.3508767	0.3232362
Minimum	1.0000	1.0000
Maximum	20.6155	19.3132
Range	19.6155	18.3132
Interquartile Range	7.0312	6.2556
Skewness	-0.263	-0.118

Table 3. Statistical analysis of experimental data

The histograms of the error distribution, shown in Fig. 13, present the distribution of error, which is the difference between the visual tracking position and double compass position.

The Q-Q plot depicted in Fig. 14. presents the performance of the observed values against the expected values. This demonstrates that the errors are approximately normally distributed centrally, with anomalies at both tail ends.

The boxplot presented in Fig. 15. visually shows the distance from 0 to the mean, which is 12.3mm and 11.3mm, for the right and left respectively. It also presents the interquartile range, which is 19.6mm and 18.3mm, for the right and left respectively, and minimum (1mm) and the maximum (20.6mm and 19.3mm) values.

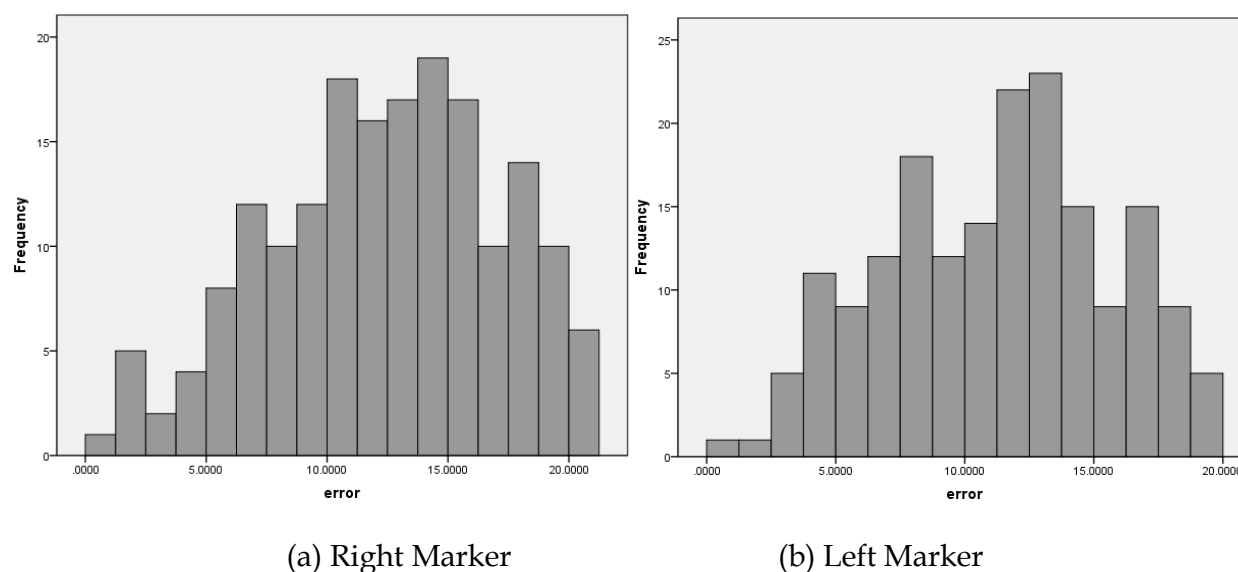


Fig. 13. Histogram of the left and right marker error

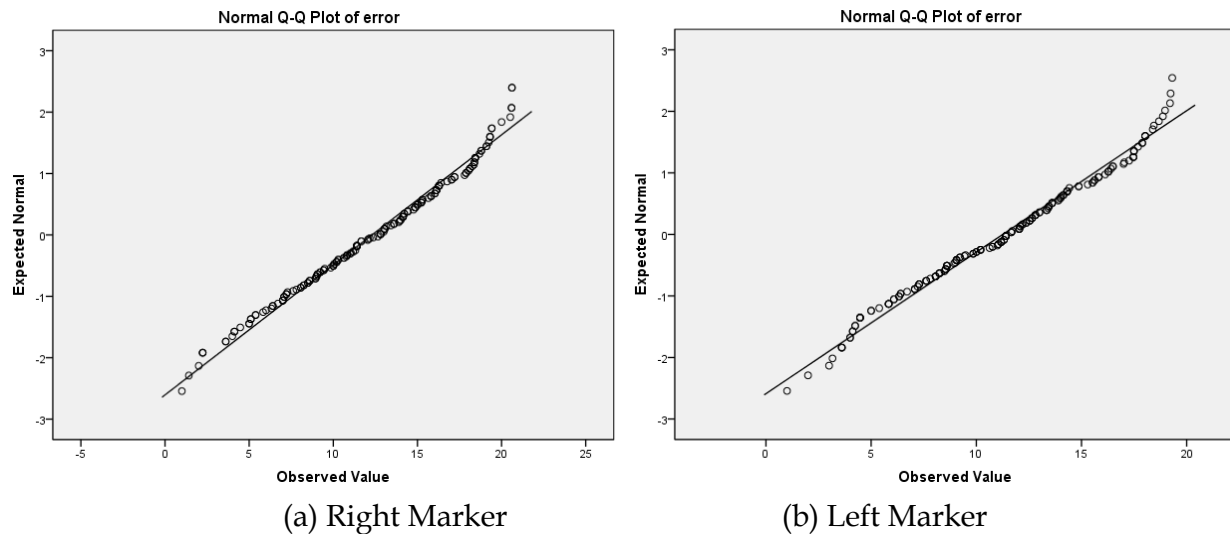


Fig. 14. Normal Q-Q Plot of Error for the Right and Left Markers

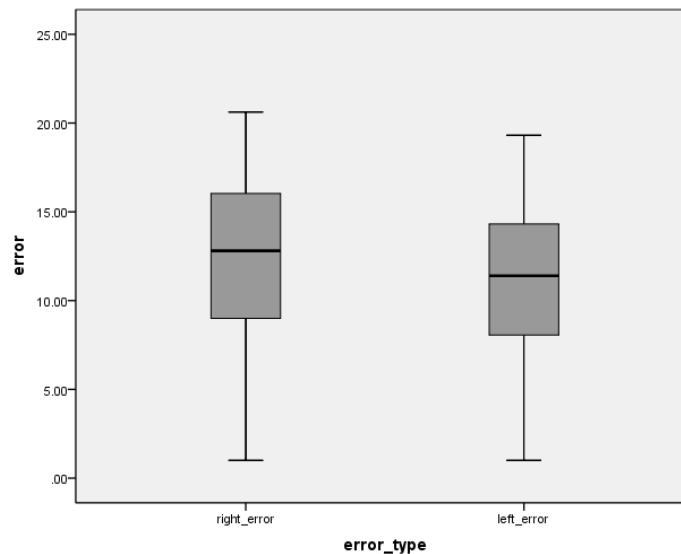


Fig. 15. Boxplot of Errors base on the Experimental Methods

5.2 Analysis using Kolmogorov-Smirnov test

Using the statistical analysis presented in the previous section, a non-parametric test is required to validate the practical effectiveness of the double compass methodology. The ideal analysis test for a non-parametric independent one-sample set of data is the Kolmogorov-Smirnov test [16] for significance. The empirical distribution function F_n for n independent and identically distributed random variables observations X_i is defined as follows:

$$F_n(x) = \frac{1}{n} \sum_{i=1}^n I_{X_i \leq x} \quad (41)$$

where $I_{X_i \leq x}$ describes the indicator function, which is equal to 1 if $X_i \leq x$ and is equal to 0 otherwise. The Kolmogorov-Smirnov statistic [16] for a cumulative distribution function $F(x)$ is as follows:

$$D_n = \sup_x |F_n(x) - F(x)| \quad (42)$$

where \sup_x describes the supremum of the set of distances. For the analysis test to be effective to reject a null hypothesis, a relatively large number of data is required.

Under the null hypothesis that the sample originates from the hypothesized distribution $F(x)$, the distribution is specified as follows:

$$\sqrt{n}D_n \xrightarrow{n \rightarrow \infty} \sup_t |B(F(t))| \quad (43)$$

where $B(t)$ describes the Brownian bridge [17]. If F is continuous, then under the null hypothesis $\sqrt{n}D_n$ converges to the Kolmogorov distribution, which does not depend on F . The analysis test is constructed by using the critical values of the Kolmogorov distribution. The null hypothesis is rejected at level α if $\sqrt{n}D_n > K_\alpha$, where K_α is calculated from the following:

$$\Pr(K \leq K_\alpha) = 1 - \alpha \quad (44)$$

It should also be noted that the asymptotic power of this analysis test is 1.

For the experimental data presented in this paper, the null hypothesis is that the distribution of error is normal with a mean value of 11.78 and a standard deviation of 4.56. Based on significance level of 0.05, a significance of 0.663 is returned using the one-sample Kolmogorov-Smirnov test (44). The strength of the returned significance value allows us to retain the null hypothesis and say that the distribution of error is normal with a mean value of 11.78 and a standard deviation of 0.663.

6. Conclusions

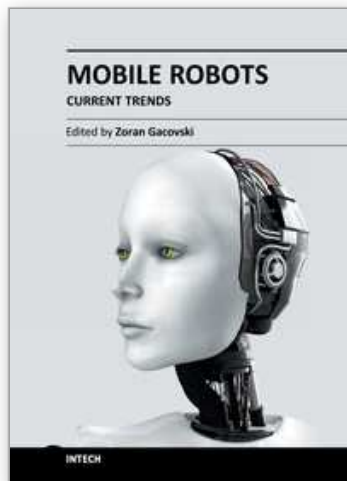
The most fundamental part of implementing a successful maneuverable non-holonomic mobile robot is accurate self-localization telemetry. The biggest concern about using a self-localization technique is the amount of computation it will require to complete the task. Ideally, having an analytical solution to position offers the benefit of a single solution, where the numeric solution has many possibilities and requires more time and computation to derive.

In this paper, three different solutions have been presented for the position of the mobile robot. The first solution presented a method where only the quadrature shaft encoder telemetry is used to solve position. However, using an accumulative method leads to the drifting of the position and orientation result, caused by slippage of the wheels or even by the limiting resolution of the shaft encoders. The second solution presented the implementation of a hybrid model using both the quadrature shaft encoders and a single, centrally placed digital compass. Modeling the maneuver configuration of the mobile robot as a six-bar linkage mechanism and using vector loop equation method to analyze the mechanism for a numeric solution was derived. The final solution presented a model that implements a dual digital compass configuration to allow an analytical solution to the purposed six-bar linkage mechanism. An analytical model was derived to resolve the numeric nature of the single compass configuration, which will allow the swift resolution of position and orientation.

The benefit of the dual compass configuration is that it offers an analytical solution to the hybrid model that utilizes quadrature shaft encoders. This paper, nevertheless, presents a novel approach where visual odometry is not possible.

7. References

- [1] Georgiou, E. *The KCLBOT Mobile Robot*. 2010; Available from: www.kclbot.com.
- [2] SRF05 *Ultra-Sonic Ranger*. Robot Electronics; Available from: <http://www.robot-electronics.co.uk/htm/srf05tech.htm>
- [3] WC-132 *WheelCommander Motion Controller*. Nu-Botics; Available from: <http://www.nubotics.com/products/wc132/index.html>
- [4] WW-01 *WheelWatcher Encoder*. Nu-Botics; Available from: <http://www.nubotics.com/products/ww01/index.html>
- [5] CMPS03 *Compass Module*. Robot Electronics; Available from: <http://www.robot-electronics.co.uk/htm/cmeps3tech.htm>
- [6] GHI *Chipworkx Module*. Available from: <http://www.ghielectronics.com/catalog/product/123>.
- [7] Nister, D., Naroditsky, O., & Bergen, J, *Visual Odometry*, in *IEEE Computer Society Conference on Computer Vision and Pattern Recognition (CVPR)*. 2004.
- [8] Frederico, C., Adelardo, M., & Pablo, A. , *Dynamic Stabilization of a Two-Wheeled Differentially Driven Nonholonomic Mobile Robot*, in *Simpósio Brasileiro de Automação Inteligente*. 2003. p. 620-624.
- [9] Hofmeister, M., Liesch, M., & Zell, A. , *Visual Self-Localization for Small Mobile Robots with Weighted Gradient Orientation Histograms*. , in *40th International Symposium on Robotics (ISR)*. 2009. p. 87-91.
- [10] Haverinen, J., & Kemppainen, A. , *Global indoor self-localization based on the ambient magnetic field*. *Robotics and Autonomous Systems*, 2009: p. 1028-1035.
- [11] Georgiou, E., Chhaniyara, S., Al-milli, S., Dai, J., & Althoefer, K. , *Experimental Study on Track-Terrain Interaction Dynamics in an Integrated Environment*, in *Proceedings of the Eleventh International Conference on Climbing and Walking Robots and the Support Technologies for Mobile Machines (CLAWAR)*. . 2008: Coimbra, Portugal.
- [12] Kolmanovsky, I.a.M., N. , *Developments in nonholonomic control problems*. *IEEE Control Systems Magazine*, 1995: p. 20-36.
- [13] Lew, A., Marsden, J., Ortiz, M. and West, M, *An Overview of Variational Integrators*. In: *Finite Element Methods: 1970's and Beyond. Theory and engineering applications of computational methods*, in *International Center for Numerical Methods in Engineering (CIMNE)*. 2004. p. 1-18.
- [14] Alexander, J.a.M., J. , *On the kinematics of wheeled mobile robots*. *The International Journal of Robotics Research*, 1989. 8: p. 15-27.
- [15] Acharyya, S.a.M., M. , *Performance of EAs for four-bar linkage synthesis*. *Mechanism and Machine Theory*, 2009. 44(9): p. 1784-1794.
- [16] Zhang, G., Wang, X., Liang, Y., and Li, J. ,, *Fast and Robust Spectrum Sensing via Kolmogorov-Smirnov Test*. *IEEE TRANSACTIONS ON COMMUNICATIONS*, 2010. 58(12): p. 3410-3416.
- [17] Hu, L., Zhu, H.,, *Bounded Brownian bridge model for UWB indoor multipath channel*. *IEEE International Symposium on Microwave, Antenna, Propagation and EMC Technologies for Wireless Communications*,, 2005: p. 1411-1414.



Mobile Robots - Current Trends

Edited by Dr. Zoran Gacovski

ISBN 978-953-307-716-1

Hard cover, 402 pages

Publisher InTech

Published online 26, October, 2011

Published in print edition October, 2011

This book consists of 18 chapters divided in four sections: Robots for Educational Purposes, Health-Care and Medical Robots, Hardware - State of the Art, and Localization and Navigation. In the first section, there are four chapters covering autonomous mobile robot Emmy III, KCLBOT - mobile nonholonomic robot, and general overview of educational mobile robots. In the second section, the following themes are covered: walking support robots, control system for wheelchairs, leg-wheel mechanism as a mobile platform, micro mobile robot for abdominal use, and the influence of the robot size in the psychological treatment. In the third section, there are chapters about I2C bus system, vertical displacement service robots, quadruped robots - kinematics and dynamics model and Epi.q (hybrid) robots. Finally, in the last section, the following topics are covered: skid-steered vehicles, robotic exploration (new place recognition), omnidirectional mobile robots, ball-wheel mobile robots, and planetary wheeled mobile robots.

How to reference

In order to correctly reference this scholarly work, feel free to copy and paste the following:

Evangelos Georgiou, Jian Dai and Michael Luck (2011). The KCLBOT: A Framework of the Nonholonomic Mobile Robot Platform Using Double Compass Self-Localisation, *Mobile Robots - Current Trends*, Dr. Zoran Gacovski (Ed.), ISBN: 978-953-307-716-1, InTech, Available from: <http://www.intechopen.com/books/mobile-robots-current-trends/the-kclbot-a-framework-of-the-nonholonomic-mobile-robot-platform-using-double-compass-self-localisat>

INTECH
open science | open minds

InTech Europe

University Campus STeP Ri
Slavka Krautzeka 83/A
51000 Rijeka, Croatia
Phone: +385 (51) 770 447
Fax: +385 (51) 686 166
www.intechopen.com

InTech China

Unit 405, Office Block, Hotel Equatorial Shanghai
No.65, Yan An Road (West), Shanghai, 200040, China
中国上海市延安西路65号上海国际贵都大饭店办公楼405单元
Phone: +86-21-62489820
Fax: +86-21-62489821

© 2011 The Author(s). Licensee IntechOpen. This is an open access article distributed under the terms of the [Creative Commons Attribution 3.0 License](#), which permits unrestricted use, distribution, and reproduction in any medium, provided the original work is properly cited.

IntechOpen

IntechOpen